Published in final edited form as:
Nature. 2017 May 24; 545(7655): 457–461. doi:10.1038/nature22358.

Rapidly star-forming galaxies adjacent to quasars at redshifts exceeding 6

R. Decarli[1], **F. Walter**[1,2,3], **B.P. Venemans**[1], **E. Bañados**[4], **F. Bertoldi**[5], **C. Carilli**[2,6], **X. Fan**[7], **E.P. Farina**[1], **C. Mazzucchelli**[1], **D. Riechers**[8], **H.-W. Rix**[1], **M.A. Strauss**[9], **R. Wang**[10], and **Y. Yang**[11]

[1]Max Planck Institut für Astronomie, Königstuhl 17, Heidelberg, 69117, Germany

[2]National Radio Astronomy Observatory, Pete V. Domenici Array Science Center, P.O. Box O, Socorro, NM, 87801, USA

[3]Astronomy Department, California Institute of Technology, MC105-24, Pasadena, CA, 91125, USA

[4]Carnegie-Princeton Fellow; The Observatories of the Carnegie Institute of Washington, 813 Santa Barbara Street, Pasadena, CA, 91101, USA

[5]Argelander Institute for Astronomy, University of Bonn, Auf dem Hügel 71, Bonn, 53121, Germany

[6]Battcock Centre for Experimental Astrophysics, Cavendish Laboratory, Cambridge CB3 0HE, UK

[7]Steward Observatory, The University of Arizona, 933 North Cherry Avenue, Tucson, AZ, 85721–0065, USA

[8]Cornell University, 220 Space Sciences Building, Ithaca, NY, 14853, USA

[9]Department of Astrophysical Sciences, Princeton University, Princeton, NJ, 08533, USA

[10]Kavli Institute of Astronomy and Astrophysics at Peking University, No.5 Yiheyuan Road, Haidian District, Beijing, 100871, China

[11]Korea Astronomy and Space Science Institute, Daedeokdae-ro 776, Yuseong-gu Daejeon 34055, Republic of Korea

Correspondence should be addressed to Roberto Decarli (decarli@mpia.de).

Author Contributions:
R.D. led the writing and analysis presented in this paper. F.W. was PI of the ALMA program that led to this discovery. F.W., B.P.V. played a central role in the project design and implementation. E.P.F. provided the clustering analysis. E.B., B.P.V., E.P.F., C.M., F.W., and H.W.R. contributed to the identification of Pan–STARRS1 quasars. X.F. provided the Hubble observations of J0842+1218. All authors have contributed in the writing of the proposal, and have reviewed, discussed, and commented on the manuscript.

Author Information:
Reprints and permissions information is available at www.nature.com/reprints.

The authors declare no competing financial interests.

Data availability statement:
The datasets generated during and/or analysed during the current study are available from the corresponding author on reasonable request. The ALMA observations presented here are part of the project 2015.1.01115.S.

Europe PMC Funders Author Manuscripts

Abstract

The existence of massive (10^{11} M_{sun}) elliptical galaxies by redshift z~4[1,2,3] (when the Universe was 1.5 billion years old) necessitates the presence of galaxies with star formation rates SFR>100 M_{sun}/yr at z>6 (corresponding to an age of the Universe of less than 1 billion years). Surveys have discovered hundreds of galaxies at these early cosmic epochs, but their star formation rates are more than an order of magnitude lower[4]. The only known examples of very high rate galaxies at z>6 are, with only one exception[5], quasar host galaxies[6,7,8,9], i.e. galaxies that host an accreting supermassive (~10^9 M_{sun}) black hole that likely affects the host properties. Here we report observations of the [CII] 158 μm line in 4 galaxies that are companions of quasars, with velocity offsets of less than 600 kilometres per second and linear offsets of less than 100 kiloparsecs. The discovery of these four galaxies was serendipitous; they are close to their companion quasars and appear bright in the far-infrared. Based upon the [CII] measurements, we estimate star formation rates of >100 M_{sun}/yr. These sources are similar to the quasar hosts in [CII] brightness, line width and implied dynamical masses, but do not show evidence for accreting supermassive black holes. Similar systems have previously been found at lower redshift[10,11,12]. We find such close companions in 4 out of 25 z>6 quasars surveyed, a fraction that needs to be accounted for in simulations[13,14]. If representative of the bright end of the [CII] luminosity function, they can account for the population of massive elliptical galaxies at z~4 in terms of cosmic space density.

We used the Atacama Large Millimeter Array (ALMA) to survey the fine-structure line of singly ionized carbon ([CII] at 158 μm) and its underlying continuum emission in high–redshift quasars in the Southern sky (declination < 15°). The [CII] line, a strong coolant of the interstellar medium, is the brightest FIR emission line at these frequencies[9,15,16]. It arises ubiquitously in galaxies, therefore it is an ideal tracer of the gas morphology and dynamics in the quasar hosts. The FIR continuum emission is associated with the dust-reprocessed light from young stars, and therefore is a measure of the dust mass and puts constraints on the SFR of the host galaxies. The parent sample includes 35 luminous (rest-frame 1450 Angstrom absolute magnitude < -25.25 mag) quasars at z>5.95 (i.e., for which the redshifted [CII] line would fall in ALMA band 6), mostly selected from the Pan–STARRS1 survey[17]; of these, 25 targets were observed with ALMA, all in single pointings with similar depth (0.6-0.9 mJy beam^{-1} per 30 km/s channel). The survey resulted in a very high detection rate (>90%) both in the continuum and line emission from the quasar host galaxies.

We searched the data cubes (in projected sky position and frequency or redshift) for additional sources in the quasar fields. The field of view of ALMA at these frequencies is about 25”, or 140 physical kpc at the mean redshift of the quasars (assuming a Lambda Cold Dark Matter cosmology with H_0=70 km/s Mpc^{-1}, Ω_m=0.3, Ω_Λ=0.7). The detection algorithm and strategy follows previous work with ALMA data[18]. We imposed a conservative significance threshold of 7-σ ($L_{[CII]}$~10^9 L_{sun}), which excludes any contamination from noise peaks. This search resulted in the discovery of four bright line-emitting sources around four of the targeted quasars, shown in Figure 1. The modest frequency differences with respect to the nearby quasars, the brightness of the lines compared to the underlying continua, and the lack of optical/near-infrared counterparts (suggesting that the companion

sources reside at high redshift, see Figure 1) imply that the detected lines are also [CII]. Furthermore, chance alignments of low-z CO emitters are expected to be >20 times rarer at these fluxes[18]. These newly-detected galaxies are also seen (at various degrees of significance) in their dust continuum emission. The line and continuum fluxes are comparable to, and in some cases even brighter than those of the quasars (see Table 1), although the companion sources are not detected in near-infrared images (sampling the rest-frame UV). Any potential accreting supermassive black holes in these companions would thus be at least one order of magnitude fainter than the quasars, or strongly obscured (see Figure 1).

Two quasars (J0842+1218 and J2100-1715) show a companion source at about 50 kpc in projected separation, with line-of-sight velocity differences of 440 km/s and 40 km/s, respectively. This suggests that the respective quasar–companion pairs lie within a common physical structure, and might even be at an early stage of interaction. The [CII] lines in these quasar companions have luminosities of ~2×10^9 L_{sun}. The marginally-resolved beam-deconvolved size of the [CII]-emitting region is ~7 kpc and ~5 kpc in these two galaxies. A Gaussian fit of the line profile yields a line width of 370 km/s and 690 km/s, comparable to those of sub-mm galaxies at lower redshift[9,19]. The implied dynamical masses of the companions within the [CII] emission regions are in the range (1-3)$\times10^{11}$ M_{sun} (see Table 1). The dust continuum is only marginally detected in the companion source of J0842+1218, while it is clearly seen in the companion of J2100-1715. The other two quasars, PJ231-20 and PJ308-21, show [CII]-bright companions at much smaller projected separation, about 10 kpc. PJ231-20's companion has very bright [CII] and FIR continuum emission, while PJ308-21's companion is fainter in the [CII] line and is only marginally detected in the continuum. Most remarkably, the [CII] emission in the companion of PJ308-21 stretches over about 25 kpc (4.5”) and about 1,000 km/s towards and beyond the quasar host, suggesting that the companion is undergoing a tidal disruption due to interaction/merger with the quasar host (see Figure 2). This extent is twice as large as the interacting groups around the sub-millimeter galaxy AzTEC-3 and the nearby UV-selected galaxy LBG-1, at z=5.3[12]. This image maps the earliest merger of massive galaxies known, 820 Myr after the Big Bang.

Modeling the dust emission as a modified black body with dust opacity index β=1.6 and dust temperature T_{dust}=47 K[20], we find that the FIR luminosities (corrected for the effects of the cosmic microwave background) of both the quasars and their companions are in the range (4-100)$\times10^{11}$ L_{sun}, with corresponding FIR-based SFRs between 80 M_{sun}/yr (PJ308-21, companion) and about 2000 M_{sun}/yr (the quasar PJ231-20; see Table 1). The dust mass[21] is M_{dust}~ 10^8-10^9 M_{sun}, or higher if the dust is not optically thin at 158 μm or its temperature is lower than assumed. For typical gas-to-dust ratios of about 100[22], this yields gas masses of 10^{10}-10^{11} M_{sun}. Figure 3a shows the [CII]-to-FIR luminosity ratio as a function of the FIR luminosity. This key diagnostic shows the contribution of the [CII] line to the cooling of the interstellar medium: in local spiral galaxies, [CII] is responsible for ~0.3% of the entire luminosity of the galaxy; in ultra-luminous infrared galaxies and high-redshift starburst galaxies, its contribution can be a factor 10 lower[9,15,23]. The quasars and their continuum-bright companions in our sample show low [CII]-to-FIR ratios (about 0.1% or less), while the companions of J0842+1218 and PJ308-21 show higher ratios (at

least >0.15%), closer to the parameter space occupied by normal star-forming galaxies in the local universe[24].

Figure 3b shows the average number of [CII]-bright galaxies observed within a given distance from a quasar in our survey. The detection of four such galaxies in 25 targeted fields exceeds the expected count rates from the (coarse) constraints (~2×10^{-4} comoving Mpc^{-3} at $L_{[CII]}>10^9$ L_{sun}) currently available on the [CII] luminosity function at $z>6$[25,26] by orders of magnitudes (the survey volume within ±1,000 km/s from the quasars is only ~400 comoving Mpc^{-3}). However, the high number of companion sources might be reconciled with the [CII] luminosity function constraints if one accounts for large-scale clustering of galaxies and quasars (such as the case of quasar–Lyman-break galaxy correlation function at z~4[27] shown in Figure 3b). Bright, high-redshift quasars therefore represent ideal signposts of the first dark matter overdensities.

Together with the quasar hosts, the newly discovered objects are the observational manifestation of rapid very early star formation in massive halos. If representative of the bright end of the [CII] luminosity function, they are sufficiently common to explain the abundance of massive galaxies (~1.8×10^{-5} comoving Mpc^{-3}) that are already in place by z~4[1]. These galaxies cannot be accounted for by the much more numerous, yet significantly less star-forming z>6 galaxies typically found in deep Hubble Space Telescope images[4], for which sensitive observations have ruled out significant dust-reprocessed emission[28,29]. A potential accreting supermassive black hole in these sources, if present, is either significantly fainter than the nearby quasars, or heavily reddened. This makes them unique objects for studying the build-up of the most massive structure in the first billion years: from an observational perspective, the absence of a blinding central lighthouse allows one to characterize these massively star-forming objects in-depth. Moreover, their interstellar medium, FIR luminosities, and implied star-formation rates are less affected by any feedback processes from the central supermassive black hole. Future observations of these sources with the James Webb Space Telescope have the promise to accurately constrain their stellar masses, a key physical parameter given the young age of the Universe. Such a measurement is very difficult in the quasar hosts given their compact emission and the enormous brightness of their central accreting supermassive black holes.

Acknowledgments

We thank J. Hennawi, Y. Shen, A. Myers, and L. Guzzo for comments on the QSO clustering. Support for R.D. was provided by the DFG priority program 1573 “The physics of the interstellar medium.”. F.W., B.V., and E.P.F. acknowledge support through ERC grant COSMIC-DAWN. R.W. acknowledge supports from the National Science Foundation of China (NSFC) grants No. 11473004, 11533001, and the National Key Program for Science and Technology Research and Development (grant 2016YFA0400703). ALMA is a partnership of ESO (representing its member states), NSF (USA), and NINS (Japan), together with NRC (Canada), NSC and ASIAA (Taiwan), and KASI (Republic of Korea), in cooperation with the Republic of Chile. The Joint ALMA Observatory is operated by ESO, AUI/NRAO, and NAOJ.

References

[1]. Straatman CMS, et al. A Substantial Population of Massive Quiescent Galaxies at z ~ 4 from ZFOURGE. Astrophys J. 2014; 783:L14.

[2]. Nayyeri H, et al. A Study of Massive and Evolved Galaxies at High Redshift. Astrophys J. 2014; 794:68.

[3]. Whitaker KE, et al. Quiescent Galaxies in the 3D-HST Survey: Spectroscopic Confirmation of a Large Number of Galaxies with Relatively Old Stellar Populations at z ~ 2. Astrophys J. 2013; 770:L39.

[4]. Bouwens RJ, et al. UV Luminosity Functions at Redshifts z ˜ 4 to z ˜ 10: 10,000 Galaxies from HST Legacy Fields. Astrophys J. 2015; 803:34.

[5]. Riechers D, et al. A dust-obscured massive maximum-starburst galaxy at a redshift of 6.34. Nature. 2013; 496:329. [PubMed: 23598341]

[6]. Bertoldi F, et al. Dust emission from the most distant quasars. Astron Astrophys. 2003; 406:L55.

[7]. Walter F, et al. A kiloparsec-scale hyper-starburst in a quasar host less than 1gigayear after the Big Bang. Nature. 2009; 457:699. [PubMed: 19194445]

[8]. Wang R, et al. Star Formation and Gas Kinematics of Quasar Host Galaxies at z ~ 6: New Insights from ALMA. Astrophys J. 2013; 773:44.

[9]. Carilli C, Walter F. Cool Gas in High-Redshift Galaxies. ARA&A. 2013; 51:105.

[10]. Omont A, et al. Molecular gas and dust around a radio-quiet quasar at redshift 4.69. Nature. 1996; 382:428. [PubMed: 8684483]

[11]. Trakhtenbrot B, et al. ALMA Observations Show Major Mergers Among the Host Galaxies of Fast-growing, High-redshift Supermassive Black Holes. Astrophys J. 2017; 836:8.

[12]. Riechers D, et al. ALMA Imaging of Gas and Dust in a Galaxy Protocluster at Redshift 5.3: [C II] Emission in "Typical" Galaxies and Dusty Starbursts ≈1 Billion Years after the Big Bang. Astrophys J. 2014; 796:84.

[13]. Narayanan D, et al. The formation of submillimetre-bright galaxies from gas infall over a billion years. Nature. 2015; 525:496. [PubMed: 26399829]

[14]. Habouzit M, et al. On the number density of `direct collapse' black hole seeds. Mon Not R Astron Soc. 2016; 463:529.

[15]. Herrera-Camus R, et al. [C II] 158 μm Emission as a Star Formation Tracer. Astrophys J. 2015; 800:1.

[16]. de Looze I, et al. The applicability of far-infrared fine-structure lines as star formation rate tracers over wide ranges of metallicities and galaxy types. Astron Astrophys. 2014; 568:62.

[17]. Bañados E, et al. The Pan-STARRS1 Distant z > 5.6 Quasar Survey: More than 100 Quasars within the First Gyr of the Universe. Astrophys J Suppl. 2016; 227:11.

[18]. Walter F, et al. ALMA Spectroscopic Survey in the Hubble Ultra Deep Field: Survey Description. Astrophys J. 2016; 833:67.

[19]. Bothwell MS, et al. A survey of molecular gas in luminous sub-millimetre galaxies. Mon Not R Astron Soc. 2013; 429:3047.

[20]. Beelen A, et al. 350 μm Dust Emission from High-Redshift Quasars. Astrophys J. 2006; 642:694.

[21]. Downes D, et al. Submillimeter spectrum and dust mass of the primeval galaxy IRAS 10214 + 4724. Astrophys J. 1992; 398:L25.

[22]. Berta S, et al. Measures of galaxy dust and gas mass with Herschel photometry and prospects for ALMA. Astron Astrophys. 2016; 587:73.

[23]. Farrah D, et al. Far-infrared Fine-structure Line Diagnostics of Ultraluminous Infrared Galaxies. Astrophys J. 2013; 776:38.

[24]. Malhotra S, et al. Far-Infrared Spectroscopy of Normal Galaxies: Physical Conditions in the Interstellar Medium. Astrophys J. 2001; 561:766.

[25]. Aravena M, et al. The ALMA Spectroscopic Survey in the Hubble Ultra Deep Field: Search for [CII] Line and Dust Emission in 6<z<8 galaxies. Astrophys J. 2016; 833:71.

[26]. Swinbank AM, et al. An ALMA survey of submillimetre galaxies in the Extended Chandra Deep Field-South: detection of [C II] at z = 4.4. Mon Not R Astron Soc. 2012; 427:1066.

[27]. Garcia-Vergara C, et al. Strong Clustering of Lyman Break Galaxies around Luminous Quasars at z~4. arXiv: 1701.01114. 2017

[28]. Bouwens RJ, et al. ALMA Spectroscopic Survey in the Hubble Ultra Deep Field: The Infrared Excess of UV-Selected z = 2-10 Galaxies as a Function of UV-Continuum Slope and Stellar Mass. Astrophys J. 2016; 833:72.

[29]. Capak P, et al. Galaxies at redshifts 5 to 6 with systematically low dust content and high [C II] emission. Nature. 2015; 522:455. [PubMed: 26108853]

[30]. Kennicutt RC, Evans NJ. Star Formation in the Milky Way and Nearby Galaxies. ARA&A. 2012; 50:531.

Europe PMC Funders Author Manuscripts

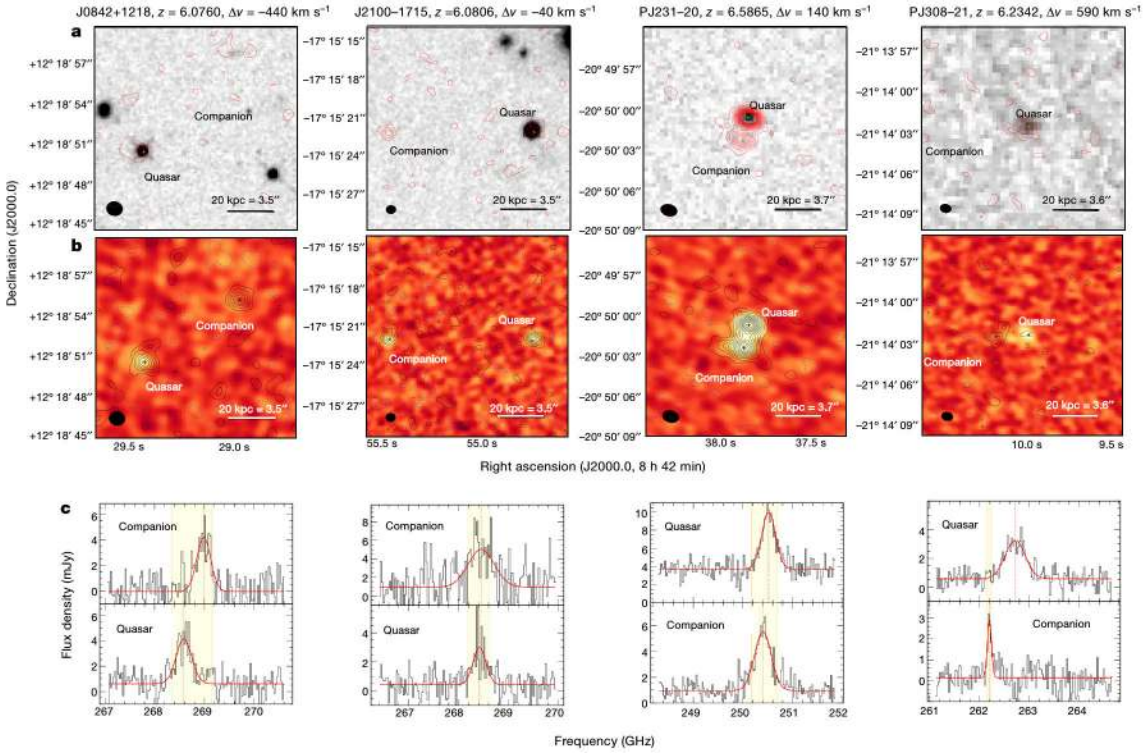

Fig. 1. Images and spectra of the quasars and their companion galaxies discovered in this study.

a) The dust continuum at 1.2 mm from ALMA is shown by red contours, which mark the ±2 σ, ±4 σ, ±6 σ, … isophotes, with σ = (81, 86, 65, 63) μJy per beam (left to right). The images were obtained with natural weighting, yielding beams of 1.20”x1.06”, 0.74”x0.63”, 1.24”x0.89” and 0.85”x0.65” (left to right), shown as black ellipses. The grey scale shows the near-infrared images of the Y- + J- (left) or J-band (otherwise) flux of the fields, obtained with (left to right) the WFC3 instrument on the Hubble Space Telescope, the LUCI camera on the Large Binocular Telescope (LBT), the SofI instrument on the European Southern Observatory (ESO) New Technology Telescope or the GROND instrument on the Max Planck Gesellschaft (MPG)/ESO 2.2-m telescope. The quasars are clearly detected in their rest-frame UV emission probed by these images, but their companion galaxies are not, implying that any potential accreting black holes, if present, are either intrinsically faint or heavily obscured. **b)** Continuum-subtracted ALMA [CII] line maps are shown as black contours, which mark the ±2 σ, ±4 σ, ±6 σ, … isophates, with σ = (0.13, 0.11, 0.15, 0.03) Jy km s^{-1} per beam (left to right). The colour scale shows the image of the 1.2-mm continuum flux density. Black ellipses are as in a. The width of each image in a and b corresponds to 15” (about 80 kpc at the redshift of the quasars). **c)** Spectra of the [CII] and underlying continuum of quasars and their companions. The channels used to create the [CII] line maps are highlighted in yellow. The spectra are modeled as a flat continuum plus a gaussian line (red lines). The velocity differences Δ v between the quasar and the companion galaxy, derived from the line fit, are listed at the top of each column. The ALMA observations were carried out in compact array configuration between January 27 and March 27 2016, in conditions of modest precipitable water vapour columns (1-2 mm). In each observations, 38-48 of the 12m antennas were used, with on-source integration times of

Europe PMC Funders Author Manuscripts

about 10 min. Nearby radio quasars were used for calibration. Typical system temperatures ranged between 70-130 K.

Europe PMC Funders Author Manuscripts

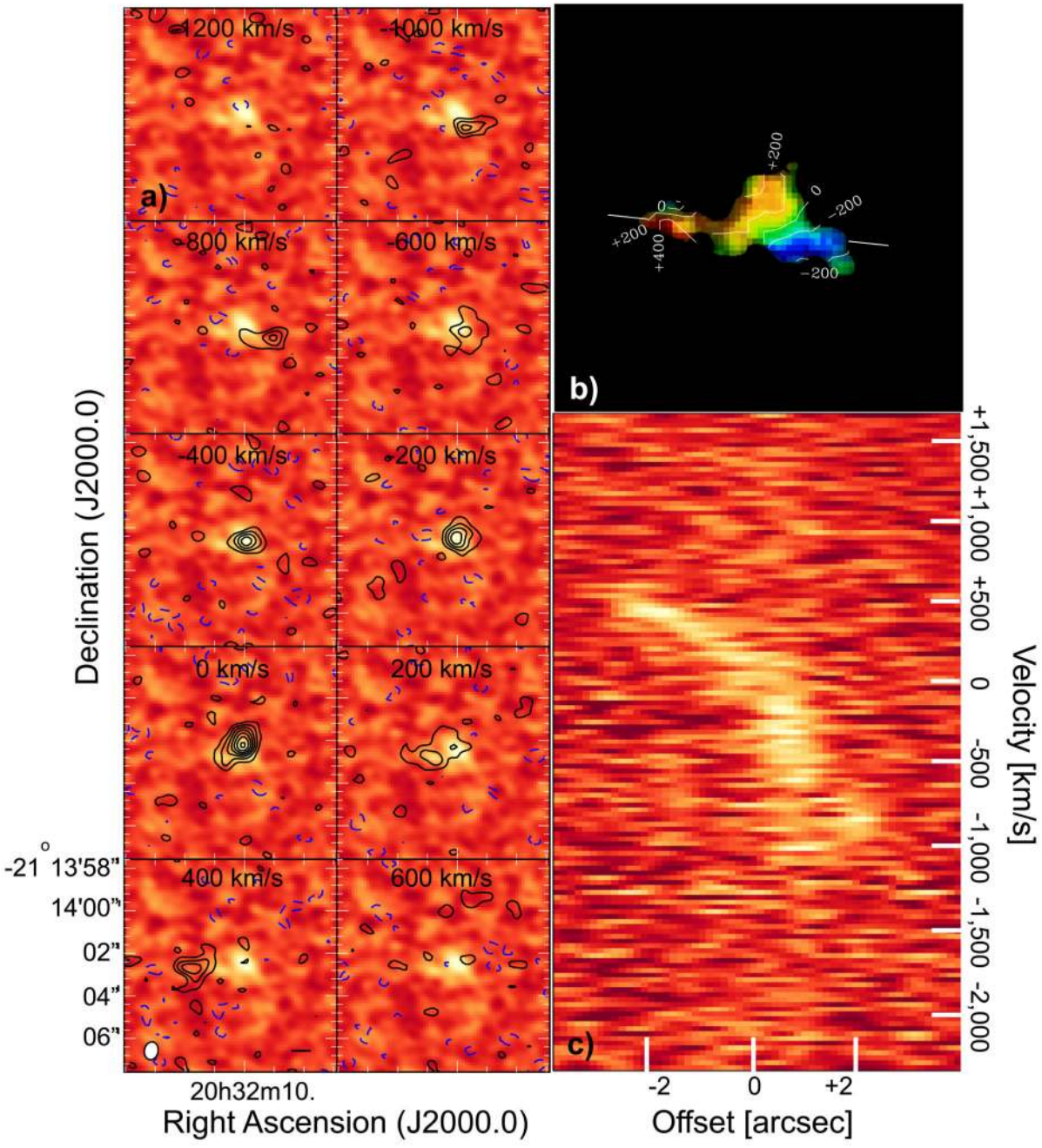

Fig. 2. Velocity structure in the system PJ308-21.

a) Continuum-subtracted [CII] channel maps of PJ308-21 and its companion (contours). The underlying continuum is shown in color. The velocity zero point is set by the quasar redshift (z=6.2342). Each panel is 10”x10” in size, corresponding to about 50 kpc x 50 kpc. Contours mark the ± 2, 4, 6, …, σ isophotes. **b)** Velocity field of PJ308-21. The isovelocity lines are marked in white (labels in km/s). The white bar marks the position at which the position-velocity diagram in panel **c)** is extracted. A clear velocity gradient is observed in the [CII] emission extending over 4.5” (~25 kpc) and >1000 km/s, connecting the

companion source in the East with the quasar host galaxy and extending even further towards the West.

Europe PMC Funders Author Manuscripts

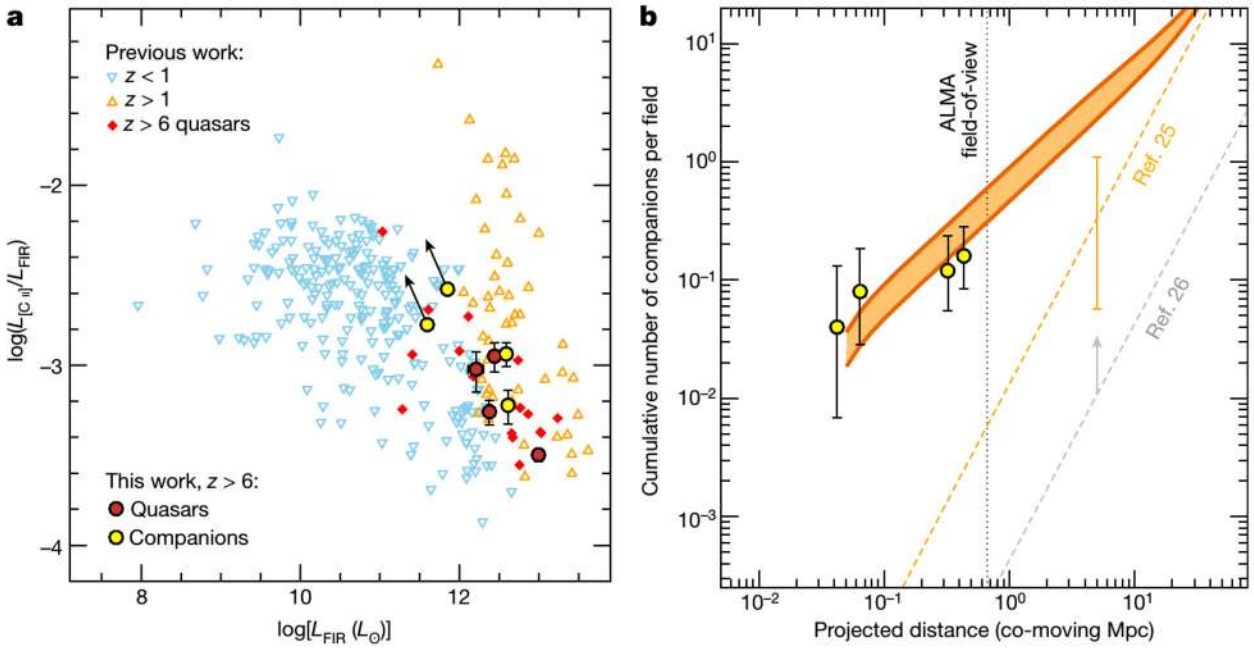

Fig. 3. Intensely star-forming galaxies in the first galactic overdensities.

a) The [CII]-to-FIR luminosity ratio, a key diagnostic of the contribution of the [CII] line to the cooling in the star-forming interstellar medium, as a function of the FIR luminosity. Sources from the literature are shown with small symbols (blue/cyan/purple for local galaxies, yellow/orange/red for high redshift sources)[5,9,23,24]. The filled symbols highlight sources at z>6, with 1-σ error bars for the sources from our study. Arrows mark the 3-σ limits. The quasars examined here appear toward the FIR-bright end of the plot, consistent with other quasars observed at these redshifts. Two of the companion sources (J2100-1715 and PJ231-20) fall in the same regime. However, two companions (J0842+1218 and PJ308-21) populate a different area of the plot, where less extreme star-forming galaxies are found. **b)** The cumulative number of [CII]-bright companion sources identified in our survey (yellow filled circles, with Poissonian 1σ uncertainties) compared with the constraints from the luminosity function set by blind-field searches of [CII] at high redshift (orange 25 and grey 26 dashed lines) as a function of the sky-projected distance from the quasars. We adopt a cylindrical volume centered on the quasar and with depth corresponding to a ±1,000 km/s difference in redshift space. The ALMA field-of-view is also shown for reference (black dotted line). There is an excess by many orders of magnitudes compared with the general field expectations; however, the observed counts can be explained if the limiting case of quasar–Lyman-break-galaxy clustering measured at z~4 is assumed. In this case, the large-scale clustering is modeled as $\xi(r)=(r_0/r)^{\gamma}$, with a scale length $r_0=8.83_{-1.51}^{+1.39}\ h^{-1}$ comoving Mpc fitted for quasar-galaxy pairs at z~4 at a fixed slope γ=2.0[27] (shaded area).

Europe PMC Funders Author Manuscripts

Table 1

Measured and derived quantities for the quasars and their companions. The spatial coordinates, [CII] fluxes, and size estimates refer to the 2D gaussian fit of the continuum-subtracted [CII] maps. The continuum fluxes are taken from the 2D gaussian fit of the continuum maps shown in Figure 1. The [CII] redshifts, line widths and relative line-of-sight velocity differences ($\Delta v_{los} = v_{comp} - v_{quasar}$) are measured from the gaussian fit of the [CII] line in the spectra. [CII] luminosities are computed as $L_{[CII]}/L_{sun} = 1.04 \times 10^{-3} F_{[CII]} \nu_{obs} D_L^2$, where $F_{[CII]}$ is the line flux in Jy km/s, ν_{obs} is the redshifted frequency of the [CII] line in GHz, and D_L is the luminosity distance in Mpc. IR luminosities are computed by integrating, between rest-frame wavelengths 3 and 1000 μm[20,30], a modified black body with T_{dust}=47 K and β=1.6, scaled to match the observed continuum flux densities. The FIR luminosity for this template is L_{FIR}=0.75 L_{IR}. The star-formation rates[16,30] are computed as $SFR_{[CII]}$ [M_{sun}/yr] = 3.0 x 10^{-9} ($L_{[CII]}$ [L_{sun}])$^{1.18}$ and SFR_{IR} [M_{sun}/yr] = 1.49 x 10^{-10} L_{IR} [L_{sun}]. The dynamical masses are computed as M_{dyn} = size $\sigma_{[CII]}^2$ / G, where σ is the gaussian width of the line, and G is the gravitational constant. We caution however that the velocity field of these galaxies might be perturbed, and that the [CII] emission is only marginally resolved in our observations.

	SDSS J0842+1218		CFHQ J2100-1715		PSO J231-20		PSO J308-21	
	Quasar	Comp	Quasar	Comp	Quasar	Comp	Quasar	Comp*
Right ascension (J2000.0)	08:42:29.43	08:42:28.95	21:00:54.70	21:00:55.45	15:26:37.84	15:26:37.87	20:32:10.00	20:32:10.17
Declination (J2000.0)	+12:18:50.4	+12:18:55.1	-17:15:21.9	-17:15:21.7	-20:50:00.8	-20:50:02.3	-21:14:02.4	-21:14:02.7
$z_{[CII]}$	6.0760 ±0.0006	6.0656 ±0.0007	6.0806 ±0.0011	6.0796 ±0.0008	6.58651 ±0.00017	6.5900 ±0.0008	6.2342 ±0.0010	6.2485 ±0.0005
m_{AB}(J)	19.78±0.01	>24.90 (3σ)	21.42±0.01	>24.80 (3σ)	19.66±0.05	>21.29 (3σ)	20.17±0.11	>21.89 (3σ)
F_{cont} [mJy]	0.87±0.18	0.36±0.12	1.20±0.15	2.05±0.27	4.41±0.16	1.73±0.16	1.34±0.21	0.19±0.06
$F_{[CII]}$ [Jy km/s]	1.61±0.21	1.96±0.26	1.37±0.14	2.55±0.44	2.91±0.20	4.15±0.49	3.12±0.29	0.66±0.13
Width [km/s]	410±80	370±70	340±70	690±150	390±50	475±75	540±55	110±30
Size [kpc]	6.0±1.8	7.0±1.4	4.0±0.7	4.6±1.0	5.0±0.8	7.7±1.6	4.8±0.9	6.4±1.7
$L_{[CII]}$ [10^9 L_{sun}]	1.55±0.20	1.87±0.24	1.32±0.13	2.45±0.42	3.13±0.22	4.47±0.53	3.10±0.29	0.66±0.13
L_{IR} [10^{11} L_{sun}]	22±5	9±3	31±4	54±7	130±5	51±5	36±6	5.2±1.7
[CII]/FIR [x 0.0001]	9.5±2.3	26±9	5.5±0.9	6.0±1.3	3.2±0.2	11.6±1.7	11±2	17±6
$SFR_{[CII]}$ [M_{sun}/yr]	210±30	260±40	170±20	360±70	480±40	730±100	480±50	77±17
SFR_{IR} [M_{sun}/yr]	340±70	140±50	470±60	800±100	1930±70	760±70	540±80	77±26
M_{dust} [10^8 M_{sun}]	2.2±0.5	1.0±0.3	3.2±0.4	5.5±0.7	13.2±0.5	5.2±0.5	3.7±0.6	0.53±0.18
M_{dyn} [10^{10} M_{sun}]	13±6	12±5	5.8±2.6	27±13	9.7±2.9	22±8	18±5	0.96±0.44
Proj. sep. [kpc]	47.7±0.8		60.7±0.7		8.4±0.6		13.8±1.0	
Δv_{los} [km/s]	-443		-41		+137		+591	

*The quoted quantities refer to the Eastern cloud in Figures 1-2. The entire [CII]-emitting arc seen in Figure 2 has a total [CII] luminosity $L_{[CII]}$~ 1.9 x 10^9 L_{sun}, and stretches over ~1000 km/s in velocity and ~25 kpc in projected physical extent.